Mathematics

https://www.aimspress.com/journal/Math

AIMS Mathematics, 11(9): 29038–29061.
DOI: 10.3934/math.20261155
Received: 13 July 2026
Revised: 10 August 2026
Accepted: 27 August 2026
Published: 09 September 2026

Research article

Exact kink and two-front solutions of an extended Benney-Luke equation via logarithmic transformations

Minghuan Liu*

School of Mathematics and Information Science, Nanchang Normal University, Nanchang, 330032, China

* **Correspondence:** Email: liuminghuan1314@sina.com; Tel: +8615727651314.

Abstract: In this paper, we investigated an extended Benney-Luke equation with second-order linear modulation, which generalizes the classical inviscid capillary-gravity shallow water wave model by introducing an additional linear second-order spatial derivative term. We first constructed the Hirota-type logarithmic transformation and derived the reduced fourth-order traveling-wave ODE, then obtained explicit single kink/antikink front solutions under the existence constraint $\frac{\alpha}{\lambda} < 0$. The method of undetermined coefficients was adopted to cross-validate the front solutions and construct four symmetric sign variants of the equal-amplitude two-front solution. Algebraic derivation showed that the interaction coefficient uniformly equals $A = 1$ for all cases, which corresponds to transparent superposition of independent wave fronts rather than nonlinear elastic soliton collision. Representative dimensionless test parameters are adopted for qualitative graphical illustration only: 3D spatiotemporal surfaces, 2D temporal sectional curves, and density contours were plotted for the velocity potential u, while supplementary figures visualized the spatially localized pulse of its spatial derivative u_x. In this work, we systematically constructed closed-form kink and two-front wavefront solutions for the linearly wave-speed modulated generalized Benney-Luke equation, filling the research gap where the literature reported only simple traveling-wave profiles.

Keywords: extended Benney-Luke equation; Hirota bilinear method; undetermined coefficient method; kink/antikink; two-front interaction
Mathematics Subject Classification: 34C25, 34C37

1. Introduction

Solitons form a special class of nonlinear waves that retain their waveforms and propagation speeds throughout evolution and collision and exhibit outstanding stability [1]. Such localized coherent structures occupy a vital position in multiple disciplines, including fluid mechanics [2–4], nonlinear optics [5–7], and plasma physics [8–10]. They can be used to model practical physical phenomena, including stable long-distance energy transfer [11, 12] and distortion-free optical signal transmission [13]. A wealth of analytical techniques have been developed to solve nonlinear wave equations for constructing soliton solutions, among which the Hirota bilinear method [14,15], Darboux transformation [16] and inverse scattering transform [17, 18] are two mainstream pure analytical approaches. Moreover, hybrid symbolic frameworks combining bilinear operators and neural networks have emerged as powerful tools to derive abundant wave structures such as lumps and breathers for high-dimensional integrable models [19]. Moreover, numerical schemes, including finite difference methods [20, 21] and spectral methods [22, 23] are widely used for quantitative wave simulation. In addition, Bäcklund transformations [24] and Darboux transformations [25] enable us to generate novel exact solutions from known analytical solutions via equivalent variable transformations.

In 1964, Benney and Luke carried out asymptotic analysis for small-amplitude long waves in three-dimensional shallow-water systems [26]. The Benney-Luke model, after one-dimensional reduction, takes the form

$$u_{tt} - u_{xx} + au_{xxxx} - bu_{xxtt} + u_{xx}u_t + 2u_x u_{xt} = 0, \tag{1.1}$$

where $u(x,t)$ denotes the velocity potential of shallow-water flow, and $\partial_t = \frac{\partial}{\partial t}$. The real parameters a and b are related to water depth and surface tension and satisfy $a - b = \sigma - \frac{1}{3}$. Here, σ denotes the Bond number, a dimensionless quantity measuring the competition between gravity and surface tension, which characterizes bidirectional propagation of capillary-gravity water waves.

Remark 1.1. In one spatial dimension, the nonlinear terms $u_t u_{xx} + 2u_x u_{xt}$ originate from the multi-dimensional nonlinear part $\Phi_t \Delta\Phi + (\nabla\Phi)_t^2$ of the Benney-Luke system. Under one-dimensional restriction $\Phi(x,t) = u(x,t)$, one has

$$\begin{aligned} \Phi_t \Delta\Phi + (\nabla\Phi)_t^2 &= u_t u_{xx} + (u_x)_t^2 \\ &= u_t u_{xx} + 2u_x u_{xt}. \end{aligned}$$

Equation (1.1) is obtained via formal asymptotic expansions starting from the full three-dimensional water-wave equations, and it is valid for the shallow-water regime of small-amplitude long waves.

Since its establishment, the classical Benney-Luke equation (1.1) has attracted extensive research attention in theoretical derivation, practical application and interdisciplinary extension. As a core mathematical model for three-dimensional shallow water waves, it has built a complete theoretical framework for nonlinear wave dynamics by integrating linear/nonlinear stability analysis, wind-driven wave evolution research and numerical verification. Li and Dai [27] adopted the dynamical system method to derive exact kink/anti-kink solutions, periodic wave solutions and bounded traveling wave solutions of Eq (1.1), and systematically analyzed the dynamical evolution characteristics of these traveling wave structures. Pego and Quintero [28] rigorously proved the nonlinear stability of line solitons governed by Eq (1.1) under weak surface tension conditions. Later, Mizumachi and Shimabukuro [29] further extended the stability analysis to two-dimensional domains and verified the linear stability of line solitary waves. Moreover, Maleewong and Grimshaw [30] modified Eq (1.1) by introducing wind forcing terms, and investigated how wind loads modulate the evolution of shallow-water wave packets.

Nevertheless, the original Benney-Luke equation is formulated under the ideal inviscid fluid hypothesis with only standard gravity-capillary dispersion terms. To enrich the model's linear dispersion structure and capture modified long-wave modulation behaviors, Yokuş, Durur, and Duran [31] proposed an extended Benney-Luke equation with an extra second-order spatial derivative term weighted by coefficient k^2, written as

$$u_{tt} - k^2 u_{xx} + a u_{xxxx} - b u_{xxtt} + c u_t u_{xx} + d u_x u_{xt} = 0, \tag{1.2}$$

where $k^2 > 0$ is a strictly positive constant modulation parameter that adjusts the linear second-order dispersion of shallow water waves, while coefficients c and d jointly regulate the nonlinear and dispersive properties of water waves. The values of these constant coefficients are determined by specific physical processes or experimental measurement data, and they exhibit distinct wave modulation behaviors under different flow environments. In reference [31], the authors constructed traveling wave solutions of Eq (1.2) via analytical expansion and put forward constraint conditions to guarantee the physical validity of obtained wave solutions. Their results demonstrated that these traveling wave structures possess soliton-like features: fixed waveform, invariant amplitude, and stable long-time propagation over unbounded spacetime.

After sorting out the research literature, we find that all studies on the extended Benney-Luke equation (1.2) merely focus on single traveling wave solutions. To date, no published work has derived the Hirota bilinear counterpart of Eq (1.2), nor has any researcher constructed two-front analytical solutions that can describe the collision interaction of multiple shallow-water solitary waves.

To fill this vacancy, we combine two analytical methods to derive its bilinear reduction, explicit kink solutions, and four families of transparent two-front solutions, with numerical visualizations to demonstrate wave structures. The contributions are summarized as follows:

(1) Derive the first Hirota bilinear counterpart of the extended model via logarithmic substitution.

(2) Obtain cross-verified kink, antikink and four symmetric sign variants of the equal-amplitude two-front transparent superposition solution.

(3) Visualize wave structures with dimensionless test parameters for morphological analysis.

2. The bilinear form and kink/antikink of Eq (1.2)

2.1. Derivation of the bilinear form for the extended Benney-Luke equation

We begin with the extended Benney-Luke equation (1.2) with second-order linear wave-speed modulation parameter k^2, which is a fully conservative modulation term without any diffusion or dissipation effect. To seek traveling wave reductions, we introduce the compound traveling variable

$$\xi = \tau x + \upsilon t,$$

and assume the velocity potential takes the traveling wave ansatz $u(x,t) = u(\xi)$, where τ (spatial scaling factor for flow pulse u_x) and υ (temporal propagation parameter) are arbitrary real constants. The real wave velocity reads $\frac{dx}{dt} = -\frac{\upsilon}{\tau}$. Substituting $u(\xi)$ and its total differential relations

$$\partial_t = \upsilon \frac{d}{d\xi}, \quad \partial_x = \tau \frac{d}{d\xi}, \quad \partial_t^n = \upsilon^n \frac{d^n}{d\xi^n}, \quad \partial_x^n = \tau^n \frac{d^n}{d\xi^n}$$

into Eq (1.2) yields a fourth-order ordinary differential equation with respect to ξ:

$$\alpha u''(\xi)+\beta u'(\xi)u''(\xi)+\lambda u^{(4)}(\xi)=0, \tag{2.1}$$

where we define three aggregated constant coefficients for conciseness:

$$\alpha=\upsilon^2-k^2\tau^2,\quad \beta=(c+d)\tau^2\upsilon,\quad \lambda=a\tau^4-b\tau^2\upsilon^2.$$

Hence, $u^{(n)}(\xi)=\dfrac{d^n u(\xi)}{d\xi^n}$ denotes the n-th order ordinary derivative of u with respect to ξ. For integrable-type solitary wave equations, a standard logarithmic transformation is adopted to eliminate the nonlinear term $\beta u'(\xi)u''(\xi)$. We set

$$u(\xi)=\frac{12\lambda}{\beta}\cdot\frac{d\ln f(\xi)}{d\xi}. \tag{2.2}$$

Substitute Eq (2.2) into the reduced fourth-order ODE (2.1) and reorganize all logarithmic derivative identities to derive the bilinear governing relation. We emphasize two critical admissibility constraints for the logarithmic transformation (2.2):

(1) Transformation singularity constraint: $\beta=(c+d)\tau^2\upsilon\neq 0$. This inequality excludes stationary wave solutions with $\upsilon=0$ and the degenerate parameter case $c+d=0$; either condition will make the logarithmic ansatz (2.2) undefined.

(2) Dispersion non-degeneracy constraint: $\lambda=a\tau^4-b\tau^2v^2\neq 0$. If $\lambda=0$, the original fourth-order traveling ODE degenerates into a second-order nonlinear equation, and no real spatially localized kink pulses can be solved from the dispersion relation (2.7).

Three critical logarithmic derivative identities associated with the one-dimensional Hirota operator are introduced to reorganize the differential system:

$$\begin{aligned}
\frac{d^2\ln f(\xi)}{d\xi^2}&=\frac{\mathrm{D}_\xi^2 f\cdot f}{2f^2},\\
\frac{d^3\ln f(\xi)}{d\xi^3}&=\frac{\mathrm{D}_\xi(\mathrm{D}_\xi^2 f\cdot f)\cdot f^2}{2f^4},\\
\frac{d^5\ln f(\xi)}{d\xi^5}&=\frac{\mathrm{D}_\xi(\mathrm{D}_\xi^4 f\cdot f)\cdot f^2}{2f^4}-\frac{3\mathrm{D}_\xi^2 f\cdot f}{f^2}\frac{\mathrm{D}_\xi(\mathrm{D}_\xi^2 f\cdot f)\cdot f^2}{f^4},
\end{aligned} \tag{2.3}$$

where

$$\begin{aligned}
&\mathrm{D}_\xi^2 f\cdot f=2ff''-2(f')^2,\\
&\mathrm{D}_\xi(\mathrm{D}_\xi^2 f\cdot f)\cdot f^2=4f(f')^3+2f^3f'''-6f^2f'f'',\\
&\mathrm{D}_\xi(\mathrm{D}_\xi^4 f\cdot f)\cdot f^2=2f^3f^{(5)}-10f^2f'f^{(4)}+4f^2f''f'''+16f(f')^2f'''-12ff'(f'')^2.
\end{aligned}$$

The general formal definition of the multivariable Hirota bilinear operator is given by [14]

$$\mathrm{D}_x^m\mathrm{D}_y^n f\cdot g=\frac{\partial^m}{\partial s^m}\frac{\partial^n}{\partial u^n}f(x+s,y+u)g(x-s,y-u)\mid_{s=0,u=0}.$$

Substituting the logarithmic transformation (2.2) and the set of logarithmic derivative identities grouped as Eq (2.3) into Eq (2.1), and eliminating the common non-zero denominator f^6, we obtain a pure polynomial differential equation of $f(\xi)$ without fractional terms:

$$\begin{aligned}&2\alpha(f')^3+\left(\alpha f^2+2\lambda ff''+8\lambda(f')^2\right)f^{(3)}\\&-ff'\left(5\lambda f^{(4)}+3\alpha f''\right)-6\lambda f'(f'')^2+\lambda f^2f^{(5)}=0,\end{aligned}\tag{2.4}$$

which can be equivalently rewritten into a compact traveling-wave reduced bilinear governing equation:

$$\alpha\mathrm{D}_\xi(\mathrm{D}_\xi^2 f\cdot f)\cdot f^2+\lambda\mathrm{D}_\xi(\mathrm{D}_\xi^4 f\cdot f)\cdot f^2=0.\tag{2.5}$$

Equations (2.4) and (2.5) are the equivalent bilinear governing relations of the extended Benney-Luke equation (1.2) under the traveling wave reduction.

2.2. Kink/antikink solutions via Hirota bilinear formalism

To construct elementary kink/antikink solutions, we employ the standard single-exponential trial function for the auxiliary function $f_1(\xi)$ in Hirota's algorithm:

$$f_1(\xi)=1+\mathrm{e}^{p_1\xi+\eta_{10}}.\tag{2.6}$$

Here, p_1 is the unknown wave number parameter to be solved, and $\eta_{10}\in\mathbb{R}$ is an arbitrary constant phase shift that controls the initial position of the kink/antikink profile.

Substitute Eq (2.6) into the bilinear constraint (2.4). Compute all derivatives $f_1', f_1'', \dots, f_1^{(5)}$ explicitly, collect all exponential terms with identical powers of $e^{p_1\xi+\eta_{10}}$, and extract the coefficient polynomial of the exponential basis. Setting the coefficient polynomial equal to zero yields the dispersion relation for p_1:

$$\alpha+\lambda p_1^2=0.\tag{2.7}$$

Solving Eq (2.7) gives two real branches of wave number:

$$p_1=\pm\sqrt{-\frac{\alpha}{\lambda}},\quad\text{subject to the existence condition }\frac{\alpha}{\lambda}<0.\tag{2.8}$$

The inequality $\frac{\alpha}{\lambda}<0$ acts as a necessary condition for generating physically meaningful localized real solitary waves for modulated shallow water wave systems. If $\frac{\alpha}{\lambda}>0$, p_1 becomes purely imaginary, which produces only non-local oscillatory waveforms without solitary wave characteristics and should be discarded in physical modeling. For the critical case $\frac{\alpha}{\lambda}=0$, the dispersion relation $\alpha+\lambda p_1^2=0$ admits only trivial zero wave number $p_1=0$, corresponding to uniform constant background flow without localized solitary wave structures; this parameter regime is also physically invalid.

Recall the logarithmic transformation relation (2.2): $u(\xi)=\frac{12\lambda}{\beta}\frac{d\ln f(\xi)}{d\xi}$. Compute the derivative $\frac{d\ln f_1}{d\xi}=\frac{p_1e^{p_1\xi+\eta_{10}}}{1+e^{p_1\xi+\eta_{10}}}$, and substitute $p_1=\pm\sqrt{-\frac{\alpha}{\lambda}}$ to obtain the unified analytical expression for kink/antikink solutions of Eq (1.2):

$$u_\pm(x,t)=\frac{\pm 12\lambda\sqrt{-\frac{\alpha}{\lambda}}\mathrm{e}^{\pm\sqrt{-\frac{\alpha}{\lambda}}(\tau x+\upsilon t)+\eta_{10}}}{\beta\left(1+\mathrm{e}^{\pm\sqrt{-\frac{\alpha}{\lambda}}(\tau x+\upsilon t)+\eta_{10}}\right)}.\tag{2.9}$$

Symbolic Maple verification code for the kink/antikink solution (2.9) is provided in Appendix A, which verifies that the residual identically vanishes under the admissible parameter constraints $\beta \neq 0, \lambda \neq 0$.

Define the constant amplitude $C = \frac{12\lambda}{\beta}\sqrt{-\frac{\alpha}{\lambda}}$. The solution simplifies to the logistic form

$$u_{\pm}(\xi) = \pm C \cdot \frac{e^{\pm\sqrt{-\frac{\alpha}{\lambda}}\xi+\eta_{10}}}{1+e^{\pm\sqrt{-\frac{\alpha}{\lambda}}\xi+\eta_{10}}}.$$

Taking the two far-field limits:

$$\lim_{\xi\to-\infty} u_{+}(\xi) = 0, \quad \lim_{\xi\to+\infty} u_{+}(\xi) = C,$$

and

$$\lim_{\xi\to-\infty} u_{-}(\xi) = -C, \quad \lim_{\xi\to+\infty} u_{-}(\xi) = 0.$$

The velocity potential $u(\xi)$ approaches two distinct constant values as $\xi \to \pm\infty$, which means this wave profile cannot be spatially localized. This feature distinguishes it from standard bright/dark solitons and confirms it belongs to the family of kink/antikink front solutions.

2.2.1. Numerical illustration of kink/antikink profiles

To visualize the spatiotemporal structure of the derived kink/antikink solutions, we adopt a concrete group of dimensionless test parameters as follows:

$$a = -1,\ b = -1,\ c = 1,\ d = 1,\ k = 3,\ \upsilon = 1,\ \tau = \frac{1}{2},\ \eta_{10} = 1.$$

Substitute these values into the definitions of α, β, λ and simplify the expression (2.9). The two explicit kink/antikink solutions are as follows:

$$u_{\pm}(x,t) = \pm\frac{3\sqrt{15}\,\mathrm{e}^{\pm\frac{2\sqrt{15}}{3}\left(t+\frac{x}{2}\right)+1}}{1+\mathrm{e}^{\pm\frac{2\sqrt{15}}{3}\left(t+\frac{x}{2}\right)+1}}.$$

$u_{+}(x,t)$ and $u_{-}(x,t)$ are monotonic step-shaped kink/antikink velocity potentials. They share the identical combined traveling coordinate $\xi = \tau x + \upsilon t$, so they possess the same propagation speed. For a fixed phase $\xi = C$, implicit differentiation gives the wave speed

$$\frac{dx}{dt} = -\frac{\upsilon}{\tau} = -2,$$

which applies equally to both profiles. The sign of the wave number $\pm\sqrt{-\frac{\alpha}{\lambda}}$ flips only the monotonic trend of the step (rising for u_{+}, falling for u_{-}) and does not alter the propagation direction of the wave front. The morphological features of these non-local step profiles are shown in Figure 1.

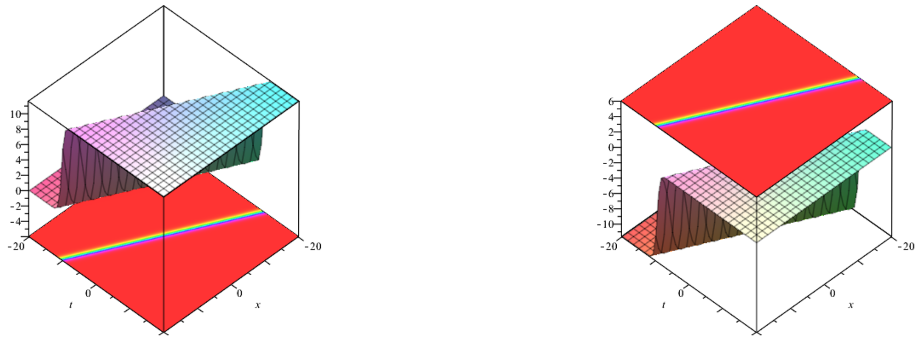

(a) Kink/antikink $u_+(x,t)$ (b) Kink/antikink $u_-(x,t)$

Figure 1. Graphical illustration of analytical kink/antikink waveforms $u_\pm(x,t)$, including 3D spatiotemporal surface and density contour plots.

Crucially, the velocity potential $u(x,t)$ cannot be regarded as a localized soliton; it merely connects two distinct constant far-field background values. The physically measurable, spatially localized solitary signal describing horizontal flow velocity is its spatial gradient

$$(u_\pm)_x = \frac{15\,\mathrm{e}^{\pm(\frac{2}{3}\sqrt{15}t+\frac{1}{3}\sqrt{15}x)+1}}{\left[1+\mathrm{e}^{\pm(\frac{2}{3}\sqrt{15}t+\frac{1}{3}\sqrt{15}x)+1}\right]^2}.$$

The bell-shaped, spatially confined pulse of u_x (plotted in Figure 2) embodies the true solitary wave feature. The preserved monotonic step shape of u alone cannot serve as evidence for solitary wave stability; the invariant amplitude and localized shape of u_x across spacetime provide valid verification of stable wave propagation.

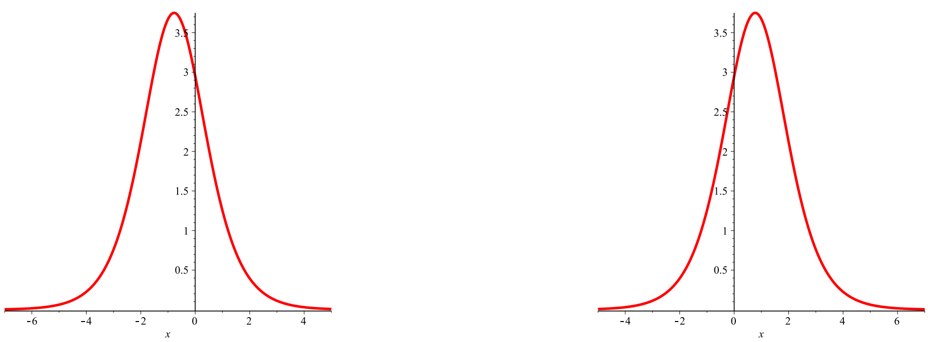

(a) $(u_+)_x$ for $t=0$ (b) $(u_-)_x$ for $t=0$

Figure 2. Graphical illustration of localized spatial pulse $(u_\pm)_x$ at fixed time $t=0$.

2.3. Supplementary discussion

2.3.1. Limiting case $k \to 0$ corresponding to the classical Benney-Luke equation

We first investigate the important limit $k \to 0$, which recovers the original classical Benney-Luke equation without the second-order modulation term $k^2 u_{xx}$. As $k \to 0$, the aggregated coefficient $\alpha = \upsilon^2 - k^2\tau^2$ converges to a positive constant υ^2. Accordingly, the fundamental existence constraint $\frac{\alpha}{\lambda} < 0$ reduces to a simpler condition $\lambda < 0$.

When $\lambda < 0$, we obtain real wave numbers $p_1 = \pm\sqrt{-\frac{\alpha}{\lambda}}$, so well-defined kink and antikink front solutions still exist for the classical Benney-Luke equation. In contrast, if $\lambda > 0$, the ratio $\frac{\alpha}{\lambda} > 0$ leads to purely imaginary wave numbers, which only produce non-localized, unbounded oscillatory waveforms without physical kink structures. All logarithmic transformation and bilinear derivation procedures derived above are fully compatible with the $k \to 0$ limit, confirming the consistency between our generalized framework and the standard Benney-Luke model.

2.3.2. Physical interpretation of the existence constraint $\frac{\alpha}{\lambda} < 0$

Recall the aggregated coefficients $\alpha = \upsilon^2 - k^2\tau^2$ and $\lambda = a\tau^4 - b\tau^2\upsilon^2$. The inequality $\frac{\alpha}{\lambda} < 0$ links the modulation strength k, wave propagation speed υ, surface tension coefficients a, b, and spatial modulation factor τ, and it defines the necessary parameter subspace supporting spatially localized shallow-water pulses u_x. This condition is well-defined only under the prerequisite $\lambda \neq 0$; two separate degenerate subcases $\alpha = 0$ and $\lambda = 0$ are analyzed in Subsections 2.3.2, where the ratio $\frac{\alpha}{\lambda}$ loses mathematical validity, and no physically relevant localized kink pulses appear within our solution framework.

2.3.3. Degenerate regimes: $\alpha = 0$ and $\lambda = 0$

(1) Case $\lambda = 0$: Setting $\lambda = 0$ reduces the fourth-order traveling-wave ordinary differential equation (2.1) to the second-order nonlinear ODE:

$$\alpha u''(\xi) + \beta u'(\xi) u''(\xi) = 0.$$

Factor the left-hand side completely to yield

$$u''(\xi) \cdot \big(\alpha + \beta u'(\xi)\big) = 0.$$

This fully factorized equation splits into two mutually exclusive solution branches governed by separate low-order equations.

(2) Case $\alpha = 0$: Substitute $\alpha = \upsilon^2 - k^2\tau^2 = 0$ into dispersion relation (2.7), we obtain $p_1 = 0$ for all non-singular $\lambda \neq 0$. This yields trivial uniform constant background flow with no transitional kink front layers.

2.3.4. Modulation parameter k and feasible parameter domain

The sign of the combined dispersion term λ fully determines how increasing k expands or shrinks the admissible parameter region satisfying $\frac{\alpha}{\lambda} < 0$; no universal monotonic shrinking trend holds for all parameter regimes:

(1) If $\lambda > 0$: The constraint requires $\alpha = \upsilon^2 - k^2\tau^2 < 0$, i.e., $k > \frac{\upsilon}{\tau}$. As k increases, the range of valid k values satisfying the inequality expands, enlarging the feasible subspace for localized solitary waves.

(2) If $\lambda < 0$: The constraint requires $\alpha = \upsilon^2 - k^2\tau^2 > 0$, i.e., $k < \frac{\upsilon}{\tau}$. As k increases, the admissible interval of k narrows, reducing the parameter range supporting real kink pulses.

Monotonic narrowing of the feasible region as k rises is exclusive to the subspace $\lambda < 0$ and is not universally valid.

3. Kink/antikink and two-front solutions via the method of undetermined coefficients

To cross-validate the kink/antikink analytical results derived from the Hirota bilinear formalism in Section 2 and systematically construct two-front interaction solutions for the extended Benney-Luke equation with second-order linear modulation, we adopt the method of undetermined coefficients as an independent analytical verification framework. This technique relies on a logarithmic ansatz for the velocity potential $u(x,t)$ and converts the original nonlinear partial differential equation (PDE) into a polynomial constraint over the auxiliary generating function $f(x,t)$. Equating coefficients of identical exponential monomials yields closed-form algebraic relations for wave parameters, which directly deliver exact kink/antikink and two-front analytical expressions.

We introduce the logarithmic variable transformation consistent with Hirota's framework:

$$u(x,t) = \frac{\partial}{\partial t}\ln f(x,t).$$

Substituting this ansatz into Eq (1.2) and expanding all partial derivatives via the chain rule produces an equation that is fifth-order in derivatives and quartic in f, written as

$$\rho_0 + \rho_1 f(x,t) + \rho_2 f^2(x,t) + \rho_3 f^3(x,t) + \rho_4 f^4(x,t) = 0, \tag{3.1}$$

where the coefficient polynomials $\rho_0, \rho_1, \rho_2, \rho_3, \rho_4$ encode all linear dispersive, wave-speed modulated, and nonlinear coupling terms of the generalized Benney-Luke equation

$$\begin{aligned}
\rho_0 &= 24af_t f_x^4 - 2(12b+c+d)f_x^2 f_t^3,\\
\rho_1 &= (6b+c)f_{xx}f_t^3 + (36b+2c+4d)f_x f_{xt} f_t^2 + (18b+2c+d)f_t f_x^2 f_{tt}\\
&\quad -36af_t f_x^2 f_{xx} - 24af_x^3 f_{xt},\\
\rho_2 &= 2f_t^3 - 2k^2 f_t f_x^2 - (6b+c)f_{xxt}f_t^2 + 8af_x f_t f_{xxx} - (12b+d)f_x f_t f_{xtt}\\
&\quad -(6b+c)f_t f_{xx} f_{tt} + 6af_t f_{xx}^2 - (12b+2d)f_t f_{xt}^2 + 12af_x^2 f_{xxt} - 2bf_x^2 f_{ttt}\\
&\quad -(12b+2c+d)f_x f_{xt} f_{tt} + 24af_x f_{xx} f_{xt},\\
\rho_3 &= k^2 f_t f_{xx} + 2k^2 f_x f_{xt} + 3bf_t f_{xxtt} - af_t f_{xxxx} - 4af_x f_{xxxt} + 2bf_x f_{xttt} - 3f_t f_{tt}\\
&\quad +(3b+c)f_{tt} f_{xxt} - 6af_{xx} f_{xxt} + bf_{xx} f_{ttt} - 4af_{xt} f_{xxx} + (6b+d)f_{xt} f_{xtt},\\
\rho_4 &= f_{ttt} - k^2 f_{xxt} + af_{xxxxt} - bf_{xxttt}.
\end{aligned} \tag{3.2}$$

All subsequent wave solution constructions are performed by specifying exponential trial forms for $f(x,t)$, substituting them into Eq (3.1), and enforcing the vanishing of all exponential monomial coefficients to solve for unknown wave parameters and interaction constants.

3.1. Kink/antikink exact solutions

3.1.1. Connection with traveling-wave reduction in Section 2

We first clarify the equivalence relation between the logarithmic ansatz here and the traveling-wave logarithmic transformation adopted in Section 2. Recall the traveling coordinate $\xi = \tau x + \upsilon t$, which gives $\partial_t = \upsilon \partial_\xi$. Substitute this into the logarithmic transformation in Section 2:

$$u = \frac{12\lambda}{\beta}\frac{d\ln f}{d\xi} = \frac{12\lambda}{\beta\upsilon}\partial_t \ln f.$$

The ansatz $u = \partial_t \ln f$ used throughout Section 3 corresponds to the compatibility condition $\frac{12\lambda}{\beta\upsilon} = 1$, which is equivalent to $\left(\frac{\upsilon}{\tau}\right)^2 = \frac{12a}{12b+c+d}$. This matching equality only emerges after imposing the traveling-wave assumption onto the full two-dimensional PDE in this section.

It should be emphasized that the undetermined coefficient method works directly on the original unreduced PDE without prior ODE simplification, and it can construct two-front interaction solutions unavailable via the single-variable bilinear method in Section 2, which justifies its role as an independent cross-verification tool.

3.1.2. Single-exponential trial function and dispersion relation

For kink/antikink structures, the standard single-exponential ansatz for the auxiliary function reads:

$$f(x,t) = 1 + \mathrm{e}^{h_1 x + m_1 t + n_1}, \tag{3.3}$$

where h_1 denotes the spatial wave number, m_1 is the temporal angular frequency, and $n_1 \in \mathbb{R}$ is an arbitrary constant phase shift governing the initial spatial position of the solitary wave.

Insert Eq (3.3) into the polynomial constraint (3.1) and group terms by identical exponential powers to generate an overdetermined algebraic system for h_1 and m_1:

$$\begin{cases} ah_1^4 - bh_1^2m_1^2 - k^2h_1^2 + m_1^2 = 0, \\ 11ah_1^4 - (11b+c+d)h_1^2m_1^2 + k^2h_1^2 - m_1^2 = 0. \end{cases} \tag{3.4}$$

Subtract the two algebraic equations to eliminate constant terms, separate terms containing h_1^4 and $h_1^2m_1^2$, and solve the resulting simplified system to obtain closed-form parametric expressions for h_1 and m_1:

$$\begin{cases} h_1 = \pm\sqrt{\dfrac{(12b+c+d)k^2 - 12a}{a(c+d)}}, \\ m_1 = \pm 2\sqrt{3}\sqrt{\dfrac{(12b+c+d)k^2 - 12a}{(12b+c+d)(c+d)}}, \end{cases} \tag{3.5}$$

with admissibility conditions $a \neq 0$, $c+d \neq 0$ and $12b+c+d \neq 0$. Substitute $f(x,t)$ into the logarithmic transformation $u(x,t) = \frac{\partial}{\partial t}\ln f(x,t)$ to obtain the unified analytical kink/antikink solution of Eq (1.2):

$$u(x,t) = \frac{m_1 \mathrm{e}^{m_1 t + h_1 x + n_1}}{1 + \mathrm{e}^{m_1 t + h_1 x + n_1}}. \tag{3.6}$$

Appendix B contains the Maple script for symbolic validation of Eq (3.6). For the traveling phase $\theta = h_1x + m_1t + n_1$, we evaluate the far-field asymptotic limits:

$$\lim_{\theta\to-\infty} u = 0, \quad \lim_{\theta\to+\infty} u = m_1.$$

Consistent with Section 2.2, this solution connects two distinct constant backgrounds $u = 0$ and $u = m_1$, which confirms it is a kink/antikink front rather than a localized bright/dark soliton.

3.1.3. Numerical illustration of kink/antikink profiles

We adopt a set of dimensionless test parameters for qualitative waveform visualization:

$$a = \frac{21}{8}, \quad b = 1, \quad c = 1, \quad d = 1, \quad k = \frac{\sqrt{15}}{2}, \quad n_1 = 1.$$

Substituting these values into Eq (3.5) recovers four distinct wave parameter pairs:

$$(h_1, m_1) = (2,3),\ (-2,3),\ (-2,-3),\ (2,-3). \tag{3.7}$$

The four corresponding kink/antikink solutions are explicitly written as:

$$u_1(x,t) = \frac{3\mathrm{e}^{2x+3t+1}}{1+\mathrm{e}^{2x+3t+1}}, \quad u_2(x,t) = \frac{3\mathrm{e}^{-2x+3t+1}}{1+\mathrm{e}^{-2x+3t+1}},$$
$$u_3(x,t) = \frac{-3\mathrm{e}^{-2x-3t+1}}{1+\mathrm{e}^{-2x-3t+1}}, \quad u_4(x,t) = \frac{-3e^{2x-3t+1}}{1+\mathrm{e}^{2x-3t+1}}.$$

Figure 3 provides graphical illustration for the four groups of analytical kink/antikink profiles $u_i(x,t)$ $(i = 1,2,3,4)$ via 3D spatiotemporal surfaces and density contour plots. Each $u_i(x,t)$ is a non-local step velocity potential, and the physically measurable localized solitary flow signal is captured by its spatial derivative $\partial_x u_i$. All four kink/antikink fronts propagate with fixed speed determined by the phase variable $\xi_i = h_i x + m_i t$; only the sign of h_i, m_i modulates the monotonic orientation of the step, without changing the magnitude of propagation velocity.

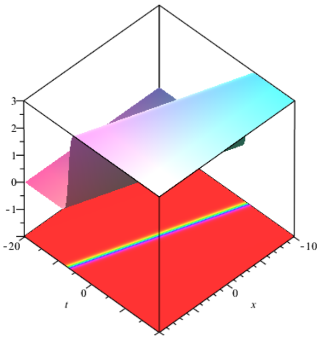

(a) Kink/antikink $u_1(x,t)$

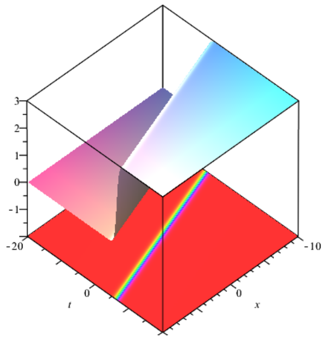

(b) Kink/antikink $u_2(x,t)$

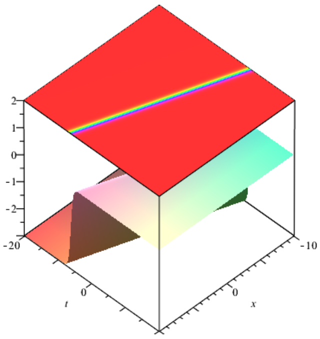

(c) Kink/antikink $u_3(x,t)$

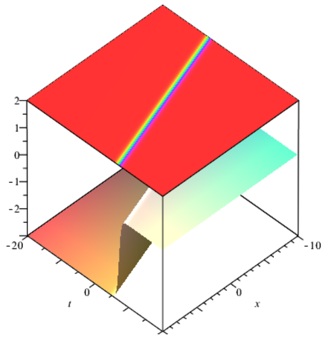

(d) Kink/antikink $u_4(x,t)$

Figure 3. Graphical illustration of four groups of analytical kink/antikink profiles $u_i(x,t)$ via 3D surfaces and contour plots.

3.2. Two-front solutions

To capture pairwise transparent superposition behaviors between two decoupled equal-amplitude kink fronts with identical wave number magnitude, we adopt the standard two-exponential Hirota ansatz for the auxiliary generating function, incorporating an undetermined interaction coefficient A to characterize cross-coupling effects between wave components:

$$f(x,t) = 1 + \mathrm{e}^{\theta_1} + \mathrm{e}^{\theta_2} + A\mathrm{e}^{\theta_1+\theta_2}, \tag{3.8}$$

where $A > 0$, and unified phase variables for two independent traveling fronts are defined as

$$\theta_1 = h_1 x + m_1 t + n_1, \quad \theta_2 = h_2 x + m_2 t + n_2.$$

Here, h_1, h_2 denote spatial wave numbers, m_1, m_2 represent temporal frequency parameters, and n_1, n_2 are arbitrary constant phase shifts determining the initial spatial positions of each kink front. The parameter pairs (h_i, m_i) $(i = 1, 2)$ strictly obey the dispersion relation Eq (3.5).

3.2.1. Symmetry invariance of the governing PDE and classification of two-front cases

We first analyze symmetry invariances of the extended Benney-Luke equation (1.2):

(1) Spatial reflection $x \mapsto -x$: The PDE remains invariant, with parameter mapping $h \mapsto -h$; propagation velocity $\upsilon = -\frac{m}{h}$ is unchanged.

(2) Time reversal $t \mapsto -t$ combined with amplitude flip $u \mapsto -u$: The equation recovers its original form, with parameter mapping $m \mapsto -m$.

As a direct algebraic consequence of Eq (3.5), the wave parameters h^*, m^* are uniquely determined by fixed model coefficients (a, b, c, d, k) only up to sign, without any free continuous spectral parameter. This implies the model does not support a continuous one-parameter family of solitary wave solutions. All four sets of sign permutations below are merely symmetric variants of an identical equal-amplitude wave pair, rather than fundamentally distinct collision modes. We restrict my discussion to the subspace $\mid h_1 \mid = \mid h_2 \mid = h^*$, $\mid m_1 \mid = \mid m_2 \mid = m^*$, and exhaust all sign permutations as four subcases:

$$\begin{cases} \text{Case 1: } (h_1, m_1, h_2, m_2) = (h^*, m^*, h^*, -m^*), \\ \text{Case 2: } (h_1, m_1, h_2, m_2) = (h^*, m^*, -h^*, m^*), \\ \text{Case 3: } (h_1, m_1, h_2, m_2) = (h^*, -m^*, -h^*, -m^*), \\ \text{Case 4: } (h_1, m_1, h_2, m_2) = (-h^*, m^*, -h^*, -m^*), \end{cases} \tag{3.9}$$

where core wave parameters are defined as

$$h^* = \sqrt{\frac{(12b+c+d)k^2 - 12a}{a(c+d)}}, \quad m^* = 2\sqrt{3}\sqrt{\frac{(12b+c+d)k^2 - 12a}{(12b+c+d)(c+d)}}.$$

Table 1 summarizes symmetry equivalence relations for the four subcases.

Table 1. Symmetry equivalence classification of four symmetric sign subcases of the single equal-amplitude two-front solution.

Symmetry transformation	Equivalent subcases	Symmetry-induced waveform characteristic
$x \mapsto -x$ spatial reflection	Case 1 $\leftrightarrow$ Case 4	Equal wave number magnitude, opposite spatial propagation velocities
$t \mapsto -t,\ u \mapsto -u$	Case 2 $\leftrightarrow$ Case 3	Opposite wave number magnitude, identical magnitude of propagation velocity

3.2.2. Derivation of interaction constant $A = 1$ and transparent superposition property

We select representative dimensionless plotting parameters:

$$a = 2,\ b = 1,\ c = 1,\ d = 1,\ k = 2,\ n_1 = 1,\ n_2 = 1,$$

which yields simplified core wave parameters

$$h^* = 2\sqrt{2}, \quad m^* = \frac{4}{7}\sqrt{42}. \tag{3.10}$$

Substitute the two-exponential trial function (3.8) into polynomial constraint Eq (3.1), collect monomials with identical exponential bases, and equate all corresponding coefficients to zero. For all four parameter configurations, the system uniformly yields the unique interaction constant $A = 1$.

When $A = 1$, the auxiliary function admits complete algebraic factorization:

$$f = \left(1 + \mathrm{e}^{\theta_1}\right)\left(1 + \mathrm{e}^{\theta_2}\right).$$

Substitute the factorized generating function into the logarithmic transformation and expand via logarithm product rule:

$$u(x,t) = \frac{\partial}{\partial t} \ln f = \frac{m_1 e^{\theta_1}}{1 + e^{\theta_1}} + \frac{m_2 e^{\theta_2}}{1 + e^{\theta_2}}. \tag{3.11}$$

Equation (3.11) clearly demonstrates that the two-front solution reduces to additive linear superposition of two independent single kink components, without any cross-coupling mixed terms of θ_1 and θ_2. No genuine nonlinear wave interaction exists between the two fronts.

Conservation of amplitude and propagation velocity

(1) **Amplitude invariance**: For single kink component $u_i = \frac{m_i e^{\theta_i}}{1+e^{\theta_i}}$, take limit $\theta_i \to +\infty$ to get $\lim\limits_{\theta_i \to +\infty} u_i = m_i$. The peak amplitude $\mid m_i \mid$ is uniquely determined by model coefficients a, b, c, d, k, independent of the second wave front; no amplitude distortion occurs during superposition.

(2) **Propagation velocity invariance**: Constant-phase trajectory satisfies $\theta_i = h_i x + m_i t + n_i = C$. Implicit differentiation gives wave speed

$$\upsilon_i = \frac{dx}{dt} \mid_{\theta_i = \text{const}} = -\frac{m_i}{h_i}.$$

Since h_i, m_i are fixed dispersion parameters without mutual coupling, the propagation speed of each front remains unchanged before, during, and after spatial overlap.

Asymptotic trajectory and zero phase shift analysis

- As $t \to -\infty$: One phase variable tends to $-\infty$ while the other approaches $+\infty$; two fronts are fully spatially separated and travel along original trajectories without perturbation.
- As $t \to +\infty$: Phase tendencies reverse, two fronts separate again after temporary overlap and fully recover their individual propagation states.

With $A = 1$, no mixed exponential term $e^{\theta_1 + \theta_2}$ exists in decomposed solution (3.11). Mathematically, zero interaction-induced phase offset appears for both kink fronts, which distinguishes this transparent superposition from classical integrable soliton collisions with nontrivial $A \neq 1$ and observable phase shifts.

3.2.3. Four symmetric two-front subcases

Case 1: Co-propagating spatial modes, opposite temporal frequencies Parameter assignment:

$$h_1 = h_2 = h^* = 2\sqrt{2}, \quad m_1 = m^*,\ m_2 = -m^*.$$

Phase variables:

$$\theta_1 = 2\sqrt{2}x + \frac{4}{7}\sqrt{42}t + 1, \quad \theta_2 = 2\sqrt{2}x - \frac{4}{7}\sqrt{42}t + 1.$$

Auxiliary function:

$$f = 1 + e^{\theta_1} + e^{\theta_2} + e^{\theta_1 + \theta_2}. \tag{3.12}$$

Corresponding two-front solution:

$$u_5(x,t)=\frac{m_1 e^{\theta_1}}{1+e^{\theta_1}}+\frac{m_2 e^{\theta_2}}{1+e^{\theta_2}}. \tag{3.13}$$

Here, $m_1>0$, $m_2<0$. The sign of temporal frequency modulates propagation velocity $\upsilon_i=-\frac{m_i}{h_i}$, generating two wavefronts traveling in opposite directions along the x-axis. All evolution proceeds with monotonically increasing physical time t, and no wave propagates backward in time. Appendix C presents Maple code to symbolically verify Eq (3.13). Figure 4 displays the 3D spatiotemporal surface and fixed-$x=4$ temporal evolution curve of $u_5(x,t)$.

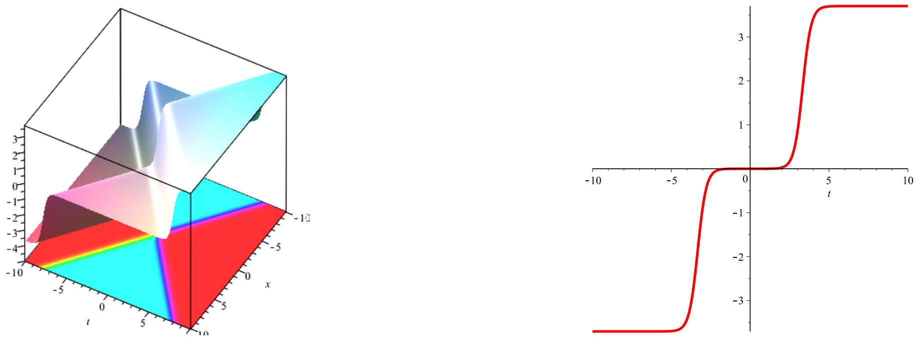

(a) Two-front $u_5(x,t)$ (b) Two-front $u_5(x,t)$ for $x=4$

Figure 4. Graphical illustration of analytical two-front symmetric variant waveform $u_5(x,t)$, containing 3D spatiotemporal surface and fixed-$x=4$ temporal curve.

Although velocity potential $u_5(x,t)$ is non-localized superposition of kinks connecting distinct constant backgrounds, the physically measurable horizontal flow corresponds to its spatial gradient $\partial_x u_5$. Direct computation yields

$$(u_5)_x=\frac{16}{7}\sqrt{21}\cdot\frac{\left(e^{\theta_1}-e^{\theta_2}\right)\left(1-e^{\theta_1+\theta_2}\right)}{\left(1+e^{\theta_1}+e^{\theta_2}+e^{\theta_1+\theta_2}\right)^2}.$$

For any finite fixed time, $\lim_{x\to\pm\infty}(u_5)_x=0$, which confirms spatially localized flow pulses. Figure 5 plots spatial sectional profiles of $(u_5)_x$ at $t=-1$ and $t=1$, showing localized pulse structures before and after front overlap.

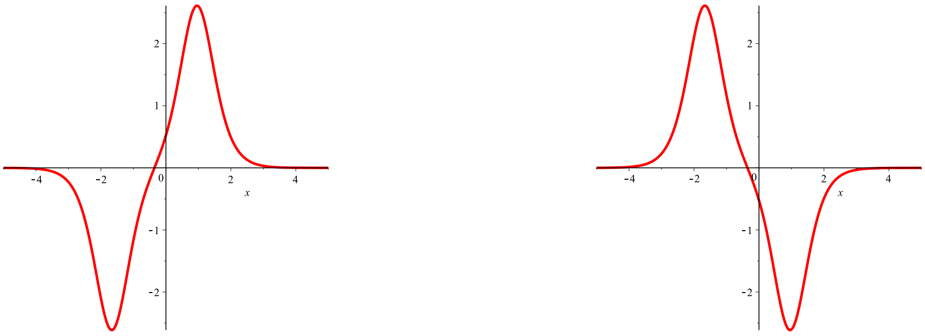

(a) $(u_5)_x$ for $t=-1$ (b) $(u_5)_x$ for $t=1$

Figure 5. Graphical illustration of spatial sectional pulses of $(u_5)_x$ at $t=\pm 1$.

Case 2: Opposite spatial modes, identical temporal frequencies Parameter assignment: $h_1 = 2\sqrt{2},\ h_2 = -2\sqrt{2},\quad m_1 = m_2 = \frac{4}{7}\sqrt{42}$. Auxiliary generating function:

$$f(x,t) = 1 + e^{2\sqrt{2}x + \frac{4}{7}\sqrt{42}t + 1} + e^{-2\sqrt{2}x + \frac{4}{7}\sqrt{42}t + 1} + e^{\frac{8}{7}\sqrt{42}t + 2}. \tag{3.14}$$

Two-front solution:

$$u_6(x,t) = \frac{m_1 e^{\theta_1}}{1+e^{\theta_1}} + \frac{m_2 e^{\theta_2}}{1+e^{\theta_2}}. \tag{3.15}$$

The two kink fronts propagate in opposite spatial directions with identical amplitude magnitude. During overlap, only temporary constructive linear superposition occurs without nonlinear phase offset. Figure 6 provides 3D surface and fixed-$x=4$ temporal curve of $u_6(x,t)$.

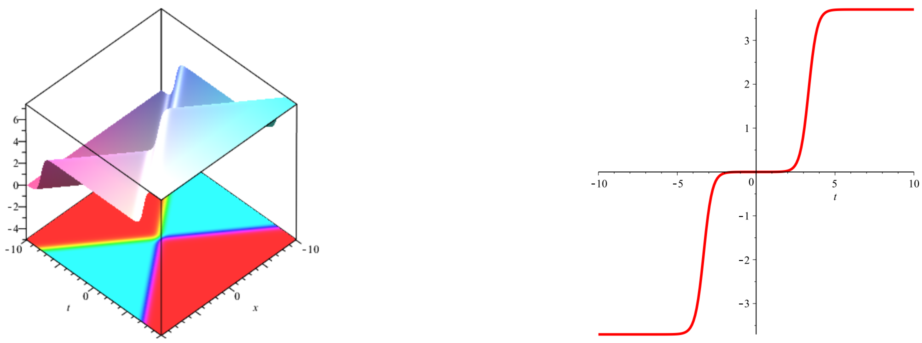

(a) Two-front $u_6(x,t)$ (b) Two-front $u_6(x,t)$ for $x=4$

Figure 6. Graphical illustration of analytical two-front symmetric variant waveform $u_6(x,t)$ with 3D surface and fixed-$x=4$ temporal section.

Case 3: Opposite spatial modes, identical negative temporal frequencies Parameter assignment:

$$h_1 = 2\sqrt{2},\ h_2 = -2\sqrt{2},\quad m_1 = m_2 = -\frac{4}{7}\sqrt{42}.$$

Auxiliary function:

$$f(x,t) = 1 + \mathrm{e}^{2\sqrt{2}x - \frac{4}{7}\sqrt{42}t + 1} + \mathrm{e}^{-2\sqrt{2}x - \frac{4}{7}\sqrt{42}t + 1} + \mathrm{e}^{-\frac{8}{7}\sqrt{42}t + 2}. \tag{3.16}$$

Two-front solution:

$$u_7(x,t) = \frac{m_1 e^{\theta_1}}{1 + \mathrm{e}^{\theta_1}} + \frac{m_2 \mathrm{e}^{\theta_2}}{1 + \mathrm{e}^{\theta_2}}. \tag{3.17}$$

Here, $m_1, m_2 < 0$, generating antikink profiles with equal amplitude magnitude. Negative temporal frequencies reverse the sign of spatial propagation velocity $\upsilon_i = -\frac{m_i}{h_i}$. This configuration describes two counter-propagating antikinks. Figure 7 displays the spatiotemporal morphology of $u_7(x,t)$.

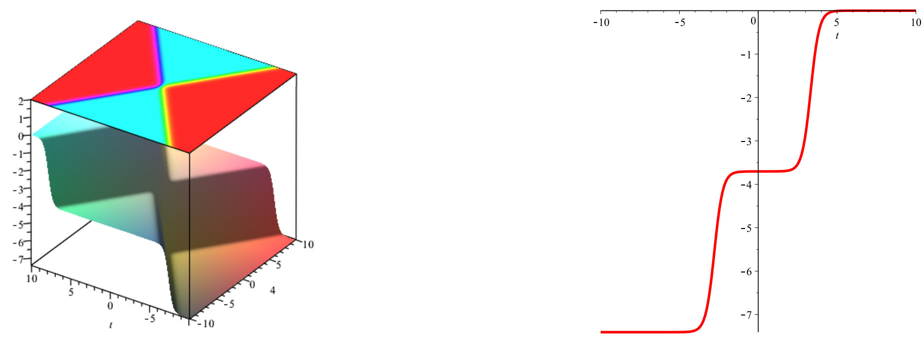

(a) Two-front $u_7(x,t)$ (b) Two-front $u_7(x,t)$ for $x = 4$

Figure 7. Graphical illustration of analytical two-front symmetric variant waveform $u_7(x,t)$ via spatiotemporal surface and temporal curve.

Case 4: Co-propagating negative spatial modes, opposite temporal frequencies Parameter assignment:

$$h_1 = h_2 = -2\sqrt{2}, \quad m_1 = \frac{4}{7}\sqrt{42},\ m_2 = -\frac{4}{7}\sqrt{42}.$$

Auxiliary function:

$$f(x,t) = 1 + \mathrm{e}^{-2\sqrt{2}x + \frac{4}{7}\sqrt{42}t + 1} + \mathrm{e}^{-2\sqrt{2}x - \frac{4}{7}\sqrt{42}t + 1} + \mathrm{e}^{-4\sqrt{2}x + 2}. \tag{3.18}$$

The corresponding two-front solution reads

$$u_8(x,t) = \frac{\frac{4\sqrt{42}}{7}\mathrm{e}^{-2\sqrt{2}x + \frac{4\sqrt{42}t}{7} + 1} - \frac{4\sqrt{42}}{7}\mathrm{e}^{-2\sqrt{2}x - \frac{4\sqrt{42}t}{7} + 1}}{1 + \mathrm{e}^{-2\sqrt{2}x + \frac{4\sqrt{42}t}{7} + 1} + \mathrm{e}^{-2\sqrt{2}x - \frac{4\sqrt{42}t}{7} + 1} + \mathrm{e}^{-4\sqrt{2}x + 2}}. \tag{3.19}$$

Amplitude magnitude and propagation speed are fully conserved throughout superposition. Figure 8 provides the graphical display of analytical two-front solution $u_8(x,t)$.

(a) Two-front $u_8(x,t)$ (b) Two-front $u_8(x,t)$ for $x = 4$

Figure 8. Graphical illustration of analytical two-front symmetric variant waveform $u_8(x,t)$, including 3D surface and fixed-$x = 4$ temporal evolution curve.

3.2.4. Remark 3.1 Structural analysis of two-front solutions and integrability discussion

For all four symmetric sign variants of equal-amplitude two-front solutions derived above, substituting the two-exponential trial function into the polynomial constraint uniquely restricts the interaction coefficient to $A = 1$. The unit interaction coefficient enables full factorization $f = (1 + e^{\theta_1})(1 + e^{\theta_2})$, which decouples two kink components and eliminates all nonlinear cross-coupling terms between wave fronts. This algebraic structure proves that the obtained two-wave solutions correspond to factorized linear superposition and transparent spatial crossing, rather than genuine nonlinear soliton collision with phase shift and waveform distortion.

Algebraic deduction on amplitude and propagation invariance proves that each separated kink front maintains fixed peak amplitude and propagation speed throughout superposition, independent of graphical demonstration. Asymptotic trajectory analysis for $t \to \pm\infty$ further demonstrates zero interaction-induced phase shift for all wave components.

Further algebraic rigidity of the wave spectrum merits explicit discussion: Since h^*, m^* are fully fixed by constant model parameters without any free adjustable spectral parameter under the present logarithmic trial-function setup, Eq (1.2) fails to admit arbitrary traveling wave parameters. The existence of freely tunable wave speeds/wave numbers is a typical characteristic of classically integrable PDEs admitting standard Hirota bilinear reduction. This spectral rigidity observed in our solution family suggests that Eq (1.2) cannot be cast into a canonical standard Hirota bilinear form via the logarithmic transformation adopted in this work. This structural feature explains why all two-front superpositions only correspond to symmetric sign permutations of a single intrinsic wave solution, and no qualitatively distinct interaction patterns emerge from this construction.

4. Conclusions

In this paper, we investigate a linearly wave-speed modulated extended Benney-Luke equation containing an extra second-order spatial modulation term, which generalizes the classical inviscid capillary-gravity shallow-water wave Benney-Luke model. This modulation adjusts only the linear wave propagation speed without introducing any dissipative or damping mechanism, fully retaining the conservative nature of the original shallow water wave system.

We first derive the reduced traveling-wave Hirota bilinear governing relation of the extended model via logarithmic transformation, and obtain closed-form kink/antikink analytical solutions subject to the necessary parameter constraint $\frac{\alpha}{\lambda} < 0$. The independent undetermined coefficient method is further adopted to cross-validate these single-front results, and systematically construct four symmetric sign variants of the equal-amplitude two-front transparent superposition solution, covering all sign permutations of the model's intrinsic wave parameter pairs.

Algebraic derivation proves that the interaction coefficient uniformly equals $A = 1$ for all configurations, which means the pairwise kink wave fronts undergo completely transparent linear superposition without any nonlinear phase shift or waveform distortion. Each individual kink front retains fixed peak amplitude and propagation velocity throughout the spatial overlap process.

We select a set of representative dimensionless test parameters to plot 3D spatiotemporal surfaces, 2D temporal sectional curves, and density contours, which intuitively demonstrate the distinct morphological difference between the non-local step-shaped velocity potential profiles and the physically measurable, spatially localized horizontal flow gradient pulses. This work fills the longstanding research gap that studies on this modulated Benney-Luke equation obtained only single traveling-wave solutions, and provides solid theoretical support for analyzing non-dissipative kink and transparent two-front wavefront structures in conservative shallow water wave systems.

It should be noted that the this analytical framework has limitations: The derived results cover only two-front solutions under the parameter constraint $\frac{\alpha}{\lambda} < 0$ and are restricted to one-dimensional scenarios. Several promising follow-up research directions are worth further exploration, including the construction of N-front ($N \geq 3$) wave solutions, two-dimensional shallow water wave dynamics, stochastic wave models with random external forcing, and coupled wave network synchronization problems inspired by multilayer and delayed multi-agent synchronization theories.

Appendices A, B, and C provide full Maple symbolic computation scripts: Appendix A verifies the single kink/antikink solution obtained via the Hirota bilinear formalism, Appendix B validates the single-front solution constructed by the undetermined coefficient method, and Appendix C confirms the exactness of the two-front superposition solution. All symbolic residuals reduce identically to zero after full simplification, rigorously certifying the validity of all analytical solutions derived in this work.

Use of Generative-AI tools declaration

The author declares they have not used Artificial Intelligence (AI) tools in the creation of this article.

Acknowledgments

The author expresses their gratitude to the referees for their insightful comments and valuable suggestions. This work is supported and funded by Jiangxi Provincial Natural Science Foundation (Grant No. 20232BAB202034), Science and Technology Research Project of Jiangxi Provincial Department of Education (Grant No. GJJ2401901) and Scientific Research Projects of Nanchang Normal University (Grant No. 24XJZR01).

Conflict of interest

The author declares no conflicts of interest in this paper.

References

1. N. J. Zabusky, M. D. Kruskal, Interaction of "solitons" in a collisionless plasma and the recurrence of initial states, *Phys. Rev. Lett.*, **15** (1965), 240–243. http://dx.doi.org/10.1103/PhysRevLett.15.240
2. D. J. Korteweg, G. De Vries, XLI. On the change of form of long waves advancing in a rectangular canal, and on a new type of long stationary waves, *Lond. Edinb. Dubl. Philos. Mag. J. Sci.*, **39** (1895), 422–443. http://dx.doi.org/10.1080/14786449508620739
3. I. Redor, E. Barthélemy, H. Michallet, M. Onorato, N. Mordant, Experimental evidence of a hydrodynamic soliton gas, *Phys. Rev. Lett.*, **122** (2019), 214502. http://dx.doi.org/10.1103/PhysRevLett.122.214502
4. K. K. Ahmed, H. H. Hussein, H. M. Ahmed, W. B. Rabie, W. Alexan, Analysis of the dynamical behaviors for the generalized Bogoyavlvensky-Konopelchenko equation and its analytical solutions occurring in mathematical physics, *Ain Shams Eng. J.*, **15** (2024), 103000. http://dx.doi.org/10.1016/j.asej.2024.103000
5. A. Hasegawa, F. Tappert, Transmission of stationary nonlinear optical pulses in dispersive dielectric fibers. I. Anomalous dispersion, *Appl. Phys. Lett.*, **23** (1973), 142–144. https://doi.org/10.1063/1.1654836
6. Y. Sun, P. Parra-Rivas, G. P. Agrawal, T. Hansson, C. Antonelli, A. Mecozzi, et al., Multimode solitons in optical fibers: A review, *Photonics Res.*, **12** (2024), 2581–2632. https://doi.org/10.1364/PRJ.531393
7. G. H. Tipu, A. Eid, H. W. A. Riaz, F. Yao, Bifurcation-Orbit classification, chaos, and nonlinear wave dynamics in (2+1)-dimensional complex coupled dispersionless system: An improved Cham method, *Math. Comput. Simul.*, **250** (2026), 905–924. http://dx.doi.org/10.1016/j.matcom.2026.07.028
8. R. B. White, B. D. Fried, F. V. Coroniti, Structure of ion acoustic solitons and shock waves in a two-component plasma, *Phys. Fluids*, **15** (1972), 1484–1490. https://doi.org/10.1063/1.1694112
9. M. E. Yahia, S. K. El-Labany, R. Sabry, W. M. Moslem, E. A. Elghmaz, Head-On collision of electron-acoustic solitons in a magnetized plasma, *IEEE Trans. Plasma Sci.*, **47** (2018), 762–769. http://dx.doi.org/10.1109/TPS.2018.2874170
10. H. Faiz, M. Abbas, T. Nazir, Y. S. Hamed, A. Birhanu, M. Alammari, Solitary wave solutions to (2+1)-dimensional coupled Riemann wave equations and their applications in mathematical physics, *J. Nonlinear Math. Phys.*, **31** (2024), 79. https://doi.org/10.1007/s44198-024-00240-x
11. D. S. Govan, W. Forysiak, N. J. Doran, Long-distance 40-Gbit/s soliton transmission over standard fiber by use of dispersion management, *Opt. Lett.*, **23** (1998), 1523–1525. https://doi.org/10.1364/OL.23.001523

12. D. D. Georgiev, J. F. Glazebrook, Thermal stability of solitons in protein α-helices, *Chaos Soliton Fract.*, **155** (2022), 111644. https://doi.org/10.1016/j.chaos.2021.111644
13. L. F. Mollenauer, K. Smith, Demonstration of soliton transmission over more than 4000 km in fiber with loss periodically compensated by Raman gain, *Opt. Lett.*, **13** (1988), 675–677. http://dx.doi.org/10.1364/OL.13.000675
14. R. Hirota, Exact solution of the Korteweg-de Vries equation for multiple collisions of solitons, *Phys. Rev. Lett.*, **27** (1971), 1192. http://dx.doi.org/10.1103/PhysRevLett.27.1192
15. T. Yin, Z. Xing, J. Pang, Modified Hirota bilinear method to (3+1)-D variable coefficients generalized shallow water wave equation, *Nonlinear Dyn.*, **111** (2023), 9741–9752. https://doi.org/10.1007/s11071-023-08356-3
16. H. W. A. Riaz, A. Alshuhail, Y. Yildirim, Soliton breathing and magnon dynamics in a ferromagnetic nanowire under time-modulated anisotropy, *Chaos Solitons Fract.*, **211** (2026), 118847. https://doi.org/10.1016/j.chaos.2026.118847
17. C. S. Gardner, J. M. Greene, M. D. Kruskal, R. M. Miura, Korteweg-de Vries equation and generalizations. VI. methods for exact solution, *Commun. Pure Appl. Math.*, **27** (1974), 97–133. https://doi.org/10.1002/cpa.3160270108
18. B. Prinari, Inverse scattering transform for nonlinear Schrödinger systems on a nontrivial background: A survey of classical results, new developments, *J. Nonlinear Math. Phys.*, **30** (2023), 317–383. https://doi.org/10.1007/s44198-023-00120-w
19. H. H. Hussein, H. Mekawey, A. Elsheikh, Exact soliton, lump, and breather solutions of the (3+1)-dimensional Jimbo-Miwa equation via the bilinear neural network method, *Sci. Rep.*, **16** (2026), 11617. https://doi.org/10.1038/s41598-026-41485-4
20. R. Courant, K. Friedrichs, H. Lewy, Über die partiellen Differenzengleichungen der mathematischen Physik, *Math. Ann.*, **100** (1928), 32–74. http://dx.doi.org/10.1007/BF01448839
21. C. Feng, C. Xie, M. Jiang, Generalized finite difference method for dynamics analysis of axially moving beams and plates, *Appl. Math. Lett.*, **166** (2025), 109526. http://dx.doi.org/10.1016/j.aml.2025.109526
22. S. A. Orszag, Accurate solution of the Orr-Sommerfeld stability equation, *J. Fluid Mech.*, **50** (1971), 689–703. https://doi.org/10.1017/S0022112071002842
23. M. Puthukkudi, C. Godavarma Raja, Mollification of Fourier spectral methods with polynomial kernels, *Math. Methods Appl. Sci.*, **47** (2024), 4911–4931. https://doi.org/10.1002/mma.9845
24. B. Fuchssteiner, A. S. Fokas, Symplectic structures, their Bäcklund transformations and hereditary symmetries, *Physica D*, **4** (1981), 47–66. http://dx.doi.org/10.1016/0167-2789(81)90004-X
25. C. Rogers, W. K. Schief, *Bäcklund and Darboux transformations: Geometry and modern applications in soliton theory*, Cambridge: Cambridge University Press, 2010. https://doi.org/10.1017/CBO9780511606359
26. D. J. Benney, J. C. Luke, On the interactions of permanent waves of finite amplitude, *J. Math. Phys.*, **43** (1964), 309–313. http://dx.doi.org/10.1002/sapm1964431309
27. J. B. Li, H. H. Dai, *On the study of singular nonlinear traveling wave equations: Dynamical system approach*, Beijing: Science Press, 2007.

28. R. L. Pego, J. R. Quintero, Two-dimensional solitary waves for a Benney-Luke equation, *Physica D*, **132** (1999), 476–496. https://doi.org/10.1016/S0167-2789(99)00058-5

29. T. Mizumachi, Y. Shimabukuro, Asymptotic linear stability of Benney-Luke line solitary waves in 2D, *Nonlinearity*, **30** (2017), 3419. https://doi.org/10.1088/1361-6544/AA7CC7

30. M. Maleewong, R. Grimshaw, Evolution of wind-generated shallow water waves in a Benney-Luke equation, *Ocean Modell.*, **200** (2026), 102659. https://doi.org/10.1016/j.ocemod.2025.102659

31. A. Yokuş, H. Durur, S. Duran, Examining wave evolution through traveling wave solutions of the extended Benney-Luke equation for a physical perspective, *Int. J. Theor. Phys.*, **64** (2025), 169. https://doi.org/10.1007/s10773-025-06021-6

Supplementary

Appendix A: Maple verification code for kink/antikink solution Eq (2.9)

The following symbolic Maple script verifies that Eq (2.9) is an exact analytical solution of the extended Benney-Luke governing equation (1.2). All calculations are carried out symbolically without fixed numerical parameters, and the residual simplifies identically to zero under $\beta \neq 0, \lambda \neq 0$.

```
restart;
# Residual of extended Benney-Luke equation (1.2)
F:=diff(u(x,t),t,t)
- k^2*diff(u(x,t),x,x)
+ a*diff(u(x,t),x,x,x,x)
- b*diff(u(x,t),x,x,t,t)
+ c*diff(u(x,t),t)*diff(u(x,t),x,x)
+ d*diff(u(x,t),x)*diff(u(x,t),x,t):

# Transformation coefficients
alpha:=upsilon^2-k^2*tau^2:
beta:=(c+d)*tau^2*upsilon:
lambda:=a*tau^4-b*tau^2*upsilon^2:

# Kink/antikink solution Eq (2.9)
u(x,t):=(12*lambda*sqrt(-alpha/lambda)
*exp(sqrt(-alpha/lambda)*(tau*x+upsilon*t)+eta[10]))
/( beta*(1+exp(sqrt(-alpha/lambda)
*(tau*x+upsilon*t)+eta[10]))):

# Compute and simplify residual
residual := simplify(F):
print("Symbolic residual after full simplification:", residual);
```

Appendix B: Maple verification code for kink/antikink solution Eq (3.6)

This Maple script provides symbolic verification for the single kink/antikink solution Eq (3.6) derived via undetermined coefficient method. Wave parameters h_1, m_1 are defined symbolically, and the simplified residual equals zero under admissible parameter ranges.

```
restart;
# Residual operator of Eq (1.2)
F:=diff(u(x,t),t,t)
- k^2*diff(u(x,t),x,x)
+ a*diff(u(x,t),x,x,x,x)
- b*diff(u(x,t),x,x,t,t)
+ c*diff(u(x,t),t)*diff(u(x,t),x,x)
+ d*diff(u(x,t),x)*diff(u(x,t),x,t):

# Symbolic wave parameters h[1], m[1]
h[1] := sqrt(-(-12*b*k^2-c*k^2-d*k^2+12*a)/(a*(c+d))):
m[1] := sqrt(-(12*(-12*b*k^2-c*k^2-d*k^2+12*a))
/((c+d)*(12*b+c+d))):

# Kink/antikink Eq (3.6)
u(x,t) := (m[1]*exp(t*m[1]+x*h[1]+n[1]))
/(1+exp(t*m[1]+x*h[1]+n[1])):

# Compute and simplify residual
residual := simplify(F):
print("Symbolic residual after full simplification:", residual);
```

Appendix C: Maple verification code for Eq (3.13)

This script verifies the transparent two-front superposition solution Eq (3.13). Representative plotting parameters are assigned at the end for numerical inspection, and the residual simplifies identically to zero after full symbolic substitution.

```
restart;
# Residual of extended Benney-Luke equation (1.2)
F := diff(u(x, t),t,t)
-k^2*(diff(u(x,t),x,x))
+a*(diff(u(x,t),x,x,x,x))
-b*(diff(u(x,t),x,x,t,t))
+c*(diff(u(x,t),t))*(diff(u(x,t),x,x))
+d*(diff(u(x,t),x))*(diff(u(x,t),x,t)):

# Unified core wave parameters h*, m*
```

```
H:= sqrt(-(-12*b*k^2-c*k^2-d*k^2+12*a)/(a*(c+d))):
M:= sqrt(-(12*(-12*b*k^2-c*k^2-d*k^2+12*a))/((c+d)*(12*b+c+d))):
h[1] := H:
m[1] := M:
h[2] := H:
m[2] := -M:

# Phase variables for two wave fronts
theta[1] := t*m[1]+x*h[1]+n[1]:
theta[2] := t*m[2]+x*h[2]+n[2]:

# Two-front additive superposition solution Eq (3.13)
u(x,t) := (m[1]*exp(theta[1]))/(1+exp(theta[1]))
+ (m[2]*exp(theta[2]))/(1+exp(theta[2])):

# Assign values to parameters a, b, c, d, k, n[1], n[2]
a := 2:
b := 1:
c := 1:
d := 1:
k := 2:
n[1] := 1:
n[2] := 1:

# Simplify residual after substitution
residual := simplify(F):
print("Symbolic residual after full simplification:", residual);
```